Eur. Phys. J. E **25**, 403–413 (2008)
DOI 10.1140/epje/i2007-10307-0

THE EUROPEAN PHYSICAL JOURNAL E

Adhesion of binary giant vesicles containing negative spontaneous curvature lipids induced by phase separation

Y. Sakuma[1], M. Imai[1,a], M. Yanagisawa[1], and S. Komura[2]

[1] Department of Physics, Ochanomizu University, Bunkyo, Tokyo 112-8610, Japan
[2] Department of Chemistry, Tokyo Metropolitan University, Tokyo 192-0397, Japan

Received 15 November 2007 and Received in final form 30 January 2008
Published online: 17 April 2008 –

Abstract. We report the adhesion of binary giant vesicles composed of two types of phospholipids, one has negative spontaneous curvature which tends to bend toward the head group and the other has zero spontaneous curvature. In a homogeneous one-phase region, the giant vesicles do not adhere to each other, whereas in a coexisting two-phase region, the giant vesicles show adhesion. A fluorescence microscope observation reveals that the adhesion takes place through the domains rich in phospholipids having negative spontaneous curvature. We propose a phase separation induced hemifusion model where two apposed monolayers of adjacent vesicles are hemifused in order to reduce the bending energy of monolayers with negative spontaneous curvature and the boundary energy between the domains and matrix. We provide a strong evidence for the hemifusion model by lipid transfer experiments.

PACS. 87.16.D- Membranes, bilayers, and vesicles – 87.16.dr Assembly and interactions – 87.14.Cc Lipids

1 Introduction

Adhesion of cell membranes is one of the elementary processes for biological phenomena such as membrane traffic, fertilization and infection by enveloped viruses. Extensive investigations have been performed to understand the membrane adhesion mechanism [1]. It has been considered that the cell adhesion is governed by the interplay of specific interactions, generic interactions and membrane elasticity. The specific interactions are lock and key forces between ligand and receptor molecules embedded in the cell membranes. A well-studied example of the ligand-receptor pair is a biotin-avidin system, which has the binding energy of $\sim 35k_{\mathrm{B}}T$. The pairs promote the adhesion of membranes by pulling together opposing membranes in closer contact.

In addition to the specific interactions, generic interactions including van der Waals, electrostatic, hydration and undulation interactions are present between lipid membranes. For two neutral membranes with distance l, the total generic interaction potential energy per unit area [2–8] is given by

$$F_{\mathrm{tot}}(l) = F_{\mathrm{hyd}}(l) + F_{\mathrm{vdW}}(l) + F_{\mathrm{und}}(l), \tag{1}$$

where the hydration energy, $F_{\mathrm{hyd}}(l)$, has the empirical form

$$F_{\mathrm{hyd}}(l) = A_h \exp(-l/\lambda_h), \tag{2}$$

with typical values of $A_h \cong 0.2\,\mathrm{J/m^2}$ and $\lambda_h \cong 0.3\,\mathrm{nm}$ [4]. The van der Waals interaction energy is expressed by

$$F_{\mathrm{vdW}}(l) = -\frac{W}{12\pi}\left[\frac{1}{l^2} - \frac{2}{(l+\delta)^2} + \frac{1}{(l+2\delta)^2}\right], \tag{3}$$

where $W \cong 10^{-22}$–$10^{-21}\,\mathrm{J}$ is the Hamaker constant and $\delta \cong 5\,\mathrm{nm}$ denotes the membrane thickness. The undulation interaction energy in the presence of membrane tension, τ, [6] is given by

$$F_{\mathrm{und}} = c_{\mathrm{und}}\frac{\tau k_{\mathrm{B}}T}{\kappa}e^{-l/l_\tau}\left(\frac{l_\tau}{l}\right)^{1/4}, \tag{4}$$

$$l_\tau = \sqrt{k_{\mathrm{B}}T/2\pi\tau}, \tag{5}$$

where κ is the bending elasticity of a single membrane and c_{und} is the dimensionless prefactor that determines the strength of the fluctuation-induced-interaction [9]. The total energy given by equation (1) yields a minimum, which causes the adhesion of membranes.

On the other hand, an intermediate hemifusion structure is considered to be formed in the first stage of the membrane fusion [10–15]. In the hemifusion state, the outer leaflets of both bilayers merge whereas the inner leaflets and the aqueous inner contents remain independent as shown in Figure 1(a). Heuvingh and co-workers showed a mixing of lipids between adhering vesicles using a fluorescence lipid transfer technique, which strongly

[a] e-mail: imai@phys.ocha.ac.jp

suggests the hemifusion state [16]. From the geometrical point of view, the hemifusion state is preferable for the lipids with negative spontaneous curvature, which tends to bend toward the head group. Actually Yang and Huang observed a periodic hemifused bilayer structure, the so-called rhombohedral phase, for a negative spontaneous curvature lipid, DPhPC (1,2-diphytanoyl-sn-glycero-3-phosphocholin) and water system [17,18]. They measured X-ray diffraction patterns from a stack of DPhPC bilayers as a function of the relative humidity. Decreasing the relative humidity, DPhPC showed a characteristic transition from lamellar bilayer to the rhombohedral structure with a space group of $R\bar{3}$, where the hemifusion structure forms a hexagonally perforated lamellar structure with ABCABC stacking as shown in Figure 1(b). The observation suggests that the two apposed monolayers with a negative spontaneous curvature merge via an hourglass-shaped structure, *i.e.* the hemifusion.

In this study, we investigate the adhesion of giant unilamellar vesicles (GUVs) by using binary GUVs composed of negative spontaneous curvature phospholipid (NP) and zero spontaneous curvature phospholipid (ZP). Here NP prefers the hourglass-like interbilayer structure when the two vesicles come into contact, whereas ZP stabilizes the binary GUVs. On the other hand, it is known that the mixture of phospholipids having different melting temperatures ($T_{\rm m}$) shows a phase separation below the miscibility transition temperature ($T_{\rm c}$). We used unsaturated and saturated acyl chains to control the melting temperatures of NP and ZP. Thus NP and ZP with different melting temperatures are homogeneously mixed above $T_{\rm c}$ and form stable spherical GUVs. Below $T_{\rm c}$, they are separated into an NP-rich phase and a ZP-rich phase, and GUVs may adhere through the NP-rich region. We use DPPE (1,2-dipalmitoyl-sn-glycero-3-phosphoethanolamine) with $T_{\rm m} = 62\,^{\circ}$C and DPhPC having no chain melting temperature between $+120$ and $-120\,^{\circ}$C as NPs. DPPE has a small phosphoethanolamine head group, whereas DPhPC has a bulky and disordered acyl tails, which gives rise to a negative spontaneous curvature. Additionally, DPPC (1,2-dipalmitoyl-sn-glycero-phosphocholine; $T_{\rm m} = 41\,^{\circ}$C) having zero spontaneous curvature is used as a reference lipid. These three phospholipids are mixed with ZPs (DOPC (1,2-dioleoyl-sn-glycero-3-phosphocholine; $T_{\rm m} = -20\,^{\circ}$C) or DPPC) to form the binary GUVs. Thus we prepared three different combinations of binary GUVs, *i.e.*, two NP/ZP pairs, DPPE/DOPC, DPhPC/DPPC and one ZP/ZP pair, DPPC/DOPC.

In order to investigate the vesicle adhesion induced by NPs, we first address spontaneous curvatures of DPPC, DPhPC and DPPE by examining the existence of the rhombohedral phase using an X-ray diffraction technique. Then we show the temperature-composition phase diagrams of the three types of the binary GUVs. With the help of the obtained phase diagrams, the adhesion behaviors are examined by a micro-manipulation technique. On the basis of the observed results, we propose a phase separation induced hemifusion model for binary GUVs containing NP. The hemifusion model is examined by the fluorescence lipid transfer experiments and the stability of the hemifusion states is discussed in terms of the free-energy calculation.

2 Experiments and methods

2.1 Commercial reagents

DPPE (> 99% purity), DPhPC (> 99% purity), DPPC (> 99% purity), and DOPC (> 99% purity) were obtained in a powder form from Avanti Polar Lipid, Inc. (Alabaster, AL). All lipids were used without further purification and were stored in chloroform at $-20\,^{\circ}$C until use. TR-DHPE (Texas Red 1,2-dihexanoyl-sn-glycero-3-phosphoethanolamine) was obtained from Molecular Probes (Eugene, OR), and used as a dye for a liquid disordered phase of membranes.

2.2 Preparation of giant vesicles

In this work, we prepared three different combinations of binary GUVs, DPPE/DOPC, DPhPC/DPPC and DPPC/DOPC. The compositions of the binary GUVs were varied from 0/100 to 100/0, although the DPPE/DOPC mixture could not form GUVs in $M_{\rm DPPE} >$ 60% region ($M_{\rm DPPE}$ is the mole fraction of DPPE). The GUVs were prepared by a gentle hydration method [19, 20]. At first we dissolved the prescribed amount of phospholipids in $10\,\mu$l of chloroform (10 mM). In order to dye the liquid disordered phase, TR-DHPE was added to the solution. TR-DHPE strongly localizes in less ordered liquid phase [21]. The solvent was evaporated in a stream of nitrogen gas and the obtained lipid film was kept under vacuum for one night to remove the remaining solvent completely. The dried lipid film was pre-warmed at $70\,^{\circ}$C, and then the sample was hydrated with 1 ml of pure water of $70\,^{\circ}$C. During the hydration process, the lipid films spontaneously form GUVs with diameters of 10–100 μm. All the experiments in this study were performed using pure water without salt.

2.3 Small-angle X-ray diffraction experiments

Following Yang and Huang's experiments, the formations of the rhombohedral phase of DPPE, DPhPC and DPPC were examined by the small-angle X-ray diffraction (SAXD) measurements. The thin film cast from the chloroform solution was dried under vacuum for one night and then chipped off from the substrate. The flakes of thin film were exposed to water vapor for one hour and then immediately sealed in the SAXD cell. The degree of hydration was controlled by keeping the hydrated sample under vacuum for 30 minutes. The SAXD measurements were performed using an apparatus (Rigaku NANO-Viewer) constructed from an X-ray rotating anode generator (18 kW, $\lambda = 1.54$ Å), a confocal mirror, and a two-dimensional position-sensitive proportional detector (Bruker AXS Hi-Star). A $1 \times 1\,{\rm mm}^2$ X-ray beam irradiates the sample via

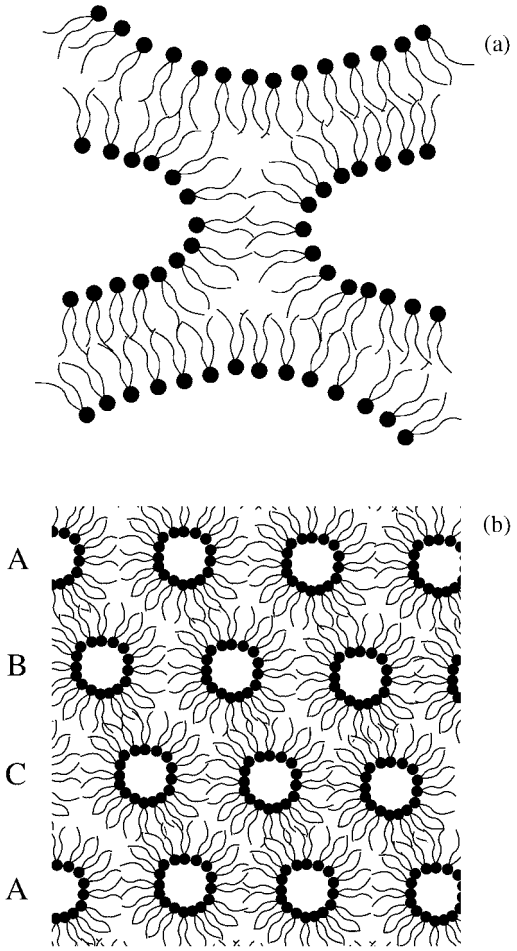

Fig. 1. (a) Schematic representation of stalk intermediate structure. (b) Hexagonally perforated lamellar structure with ABCABC stacking (rhombohedral structure with $R\bar{3}$ space group). Here we shifted the positions of holes in B and C layers to show ABCABC sequence clearly. Actual arrangement of holes is identical with the face centered cubic lattice.

pinhole collimator with three-slit system and the sample to detector distance is about 0.80 m, which covers the magnitude of the scattering vector $q = 4\pi \sin\theta/\lambda$ range from 0.03 to 0.30 Å^{-1}. All SAXD measurements were performed at 25 °C. The obtained scattering patterns were corrected for the nonuniformity, image distortion of the detector, background scattering and then circularly integrated to obtain the one dimensional profile.

2.4 Phase diagrams

We prepared three types of binary vesicles with various compositions, DPhPC/DPPC = 0/100, 5/95, 10/90, 20/80, 30/70, 40/60, 50/50, 60/40, 70/30, 80/20, 90/10, 100/0, DPPE/DOPC = 0/100, 10/90, 20/80, 30/70, 40/60, 50/50, 60/40, and DPPC/DOPC = 0/100, 20/80, 40/60, 60/40, 80/20, 100/0. The binary GUV suspension was put on a glass plate with a silicon rubber spacer having the thickness of 0.5 mm, and then sealed with a cover glass immediately. This sample cell was set on the temperature control stage (Carl Zeiss) with ±0.2 °C of accuracy. We observed the phase separation process using an inverted confocal microscope (Carl Zeiss, LSM 5) with either the laser scanning mode or the Hg lamp mode. To avoid the domain formation before the observation, we kept the sample temperature above the melting temperature of the phospholipids. For the observation of the phase separation behavior, we decreased the temperature from the one-phase region (60 °C) to the coexisting two-phase region (10 °C) with a step of 5 °C. At each temperature we equilibrated the sample for 5 minutes and then examined the formation of domains by the fluorescence microscope observation. We performed similar experiments for the binary GUVs and determined the phase separation curve. To avoid the photo-oxidation, we paid special attention to minimize the exposure time of light.

2.5 Adhesion experiments

The adhesive nature of GUVs was examined by a micromanipulation technique. A GUV with the radius of 10–40 μm was weakly aspirated by a micro-pipette (Eppendorf, Vacu Tip with the internal diameter, D_p, of 15 μm). We controlled the suction pressure at $P \sim 3$ Pa during the adhesion tests, which was monitored by a pressure transducer (Varlidyne, DP-15). The membrane tension, τ, at this suction pressure can be calculated by an expression [22]

$$\tau = PD_\text{p}/4(1 - D_\text{p}/D_\text{v}), \tag{6}$$

where D_v is the spherical vesicle diameter exterior to the pipette. In our adhesion experiments the calculated tension was in the region of 1.4–4.5 $\times$ 10^{-2} mN/m. The effect of tension on the membranes is well investigated [23] and is classified into low- and high-tension regions. In the low-tension region (10^{-3}–0.5 mN/m), the vesicle surface increases by smoothing of thermal vesicle shape fluctuations, whereas in the high-tension region (> 0.5 mN/m) direct surface stretch in area per lipid molecule becomes significant. Thus in our adhesion experiments, the vesicle membrane fluctuates around the spherical shape, which causes repulsive interaction to the adjacent membranes, or the so-called undulation repulsive force [24]. Thus in order to achieve the adhesion of vesicles in the low-tension region, the strong adhesion force is required.

Micro-manipulators (Narishige, MMO-202ND and MN-4) with a micro-injector (Narishige, IM-9B and IM-9C) system were used for positioning of the micropipettes. We applied the almost same tension ($\sim$ 3 Pa) to the two manipulated vesicles. Both of the aspirated GUVs were contacted each other for 2–3 seconds and then we pulled the micro-pipettes away from the contact position to examine whether the adhesion takes place or not. Adhesion test processes were monitored by a fluorescence microscope (Carl Zeiss, Akioskop) with a long-distance objective and recorded by a CCD camera (Carl Zeiss, Axio Cam). For the non-adhesion case, the contacted vesicles are separated by pulling the micro-pipette

away as shown in Figure 2(a). On the other hand, for the adhesion case, the contacting vesicles leave from the one side of the micro-pipette and keep contact as shown in Figure 2(b). We carried out 5 adhesion trials at each measuring point. When all trials at the measuring point showed adhesion or non-adhesion, we defined the point as adhesion point or non-adhesion point, respectively. Otherwise, we called the point as the boundary point. The adhesion measurements were performed with descending temperature, which agrees with the procedure of the phase diagram construction. The adhesion behaviors were reversible against the temperature, although they had small hysteresis of $\sim 5\,^{\circ}\mathrm{C}$.

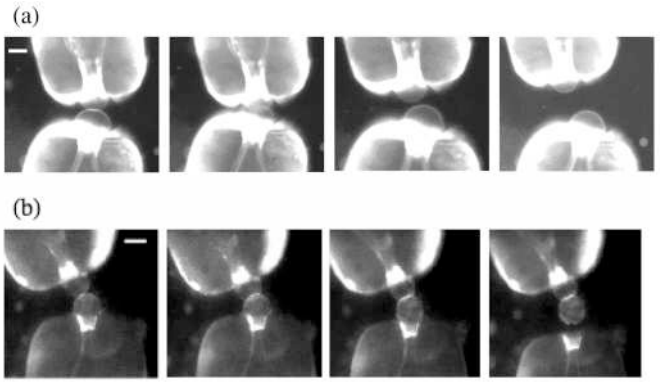

Fig. 2. Non-adhesion (a) and adhesion (b) behaviors observed in adhesion experiments. Scale bars indicate $15\,\mu$m.

2.6 Lipids transfer experiments

In order to examine the hemifusion state, we performed the fluorescence lipid transfer experiments. First, we prepared a cell with two chambers. The two chambers, a stock chamber and an observation chamber, are separated by a bank with a narrow channel. The fluorescence labeled and the non-labeled vesicles were placed in the stock chamber and the observation chamber, respectively. One of the non-labeled vesicles was held by a micro-pipette and transferred to the observation chamber through the narrow channel. In the observation chamber, a labeled vesicle and a non-labeled vesicle were brought into close proximity by the micro-manipulation technique. We observed the transfer of fluorescent signal to the non-labeled vesicle by means of the fluorescence microscope (Carl Zeiss, Akioskop) with the long-distance objective. In the lipid transfer experiments, we used giant multi-lamellar vesicles (GMVs) for the non-labeled vesicle because unilamellar vesicles are too weak to hold on the top of a micropipette during a long movement from the stock chamber to the observation chamber through the narrow channel by the micro-manipulation technique. We confirmed by the fluorescence microscope observation that the phase separation of the inner bilayers does not affect that of the outer bilayer.

3 Results

3.1 Spontaneous curvatures of lipids

First we address the spontaneous curvatures of DPPC, DPhPC and DPPE by examining the existence of the rhombohedral phase using the X-ray diffraction technique as reported by Yang and Huang [17,18]. In this study we examined the lamellar to rhombohedral transition for three phospholipids, DPPC with zero spontaneous curvature, and DPhPC and DPPE with negative spontaneous curvatures. The effect of the hydration on SAXD patterns of DPPC sample at $25\,^{\circ}\mathrm{C}$ are shown in Figure 3(a). The DPPC sample exposed to water vapor for 1 hour showed a typical diffraction pattern of the lamellar structure. After the vacuum treatment for 30 minutes, the DPPC sample kept the lamellar structure, although the lamellar peaks were shifted to the high-q side and the intensity ratio of the first peak to the second peak decreased considerably. Since the bilayer has a thickness of 50 Å, the thickness of the water layer was decreased from 11.5 Å to 7 Å by the vacuum treatment in this case. We performed similar experiments for two NPs, DPhPC and DPPE. Sufficiently hydrated DPhPC and DPPE samples showed typical diffraction patterns for the lamellar phase as shown in Figures 3(b) and (c), respectively. By vacuum treatment for 30 minutes, several new diffraction peaks appeared in both of the SAXD profiles. The peak positions predicted by the rhombohedral structure with the space group of $R\bar{3}$ are marked by the triangles in Figures 3(b) and (c). Unfortunately the intensities of some peaks in the q range from 0.15 to $0.20\,\text{Å}^{-1}$ were obscure, because the samples had many defects. We summarize the new diffraction peaks of DPhPC and DPPE samples in Tables 1 and 2, respectively, with the indexation for the $R\bar{3}$ space group. The spacing $d_{h,k,l}$ can be expressed by the unit cell dimensions, a and c, as

$$\frac{1}{d_{h,k,l}^2} = \frac{4}{3}\frac{(h^2+hk+k^2)}{a^2} + \frac{l^2}{c^2}\,. \tag{7}$$

The pronounced peak positions in the q range of 0.05 to $0.15\,\text{Å}^{-1}$ are consistent with the space group of $R\bar{3}$. It should be noted that by the subsequent vapor treatment, the rhombohedral phase transformed into the lamellar phase and this rhombohedral $\leftrightarrow$ lamellar transition was reversible against the degree of hydration. From these results we consider that DPhPC and DPPE tend to form an hourglass-like structure by the reduction of bilayer distance, indicating that the both lipids have negative spontaneous curvatures.

3.2 Phase behavior of binary vesicles

Next we investigate phase diagrams of binary GUVs composed of NP and ZP. It is known that a binary system composed of phospholipids having a high T_{m} and a low T_{m} undergoes a phase separation between the two melting temperatures [21]. At high temperature, a binary lipid

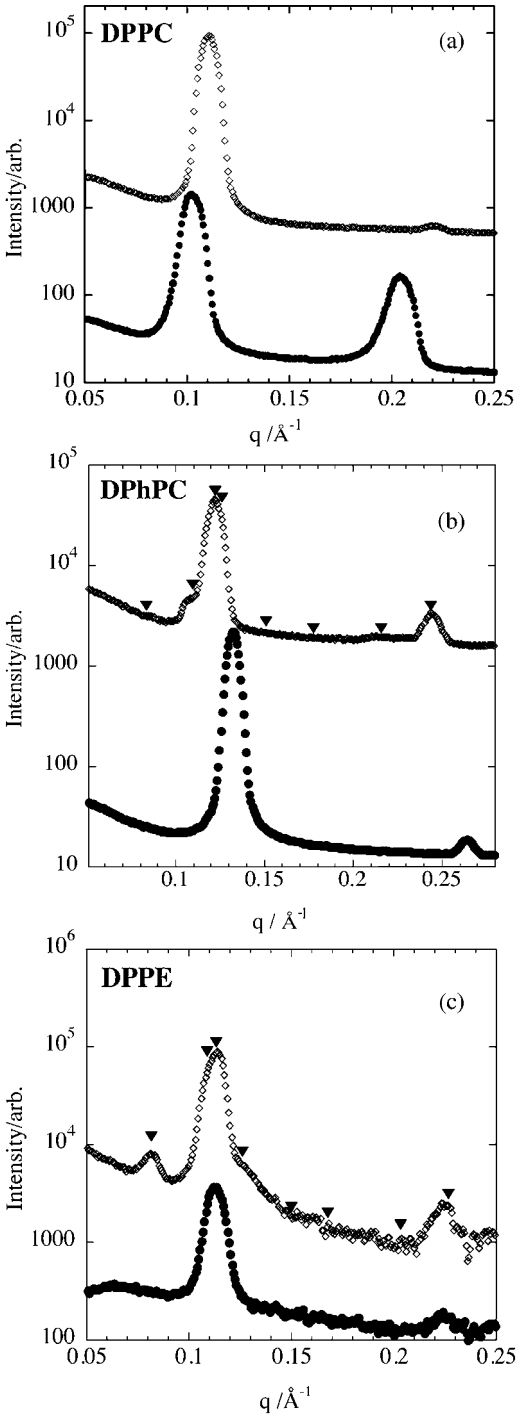

Fig. 3. Effect of degree of hydration on SAXD patterns at 25 °C. (a) DPPC, (b) DPhPC and (c) DPPE; closed circle profile: sufficiently hydrated sample, open diamond profile: after vacuum treatment for 30 min. Triangles in (b) and (c) indicate predicted peak positions from $R\bar{3}$ symmetry.

mixture is in a single uniform liquid phase, and by decreasing the temperature, the system separates into the coexisting two phases. We examined three binary systems, DPhPC/DPPC ($T_{\rm m}$ = 41 °C), DPPE (62 °C)/DOPC (−20 °C), and DPPC/DOPC. DPhPC does not exhibit the chain melting temperature between +120 °C and

Table 1. Summary of SAXD peaks of DPhPC after the vacuum treatment for 30 min. Dashes denote that definite peak was not observed.

q (Å^{-1})	$d_{\rm obs}$ (Å)	$h\ k\ l$	$d_{\rm cal}$ (Å)	a (Å)	c (Å)
0.086	73.06	1 0 1	75.54	100.21	
0.108	58.18	0 1 2	57.65	99.87	
0.122	51.50	0 0 3	51.50		154.5
-		1 1 0	50.00		
-		0 2 1	41.69		
-		1 0 4	35.28		
0.214	29.36	0 1 5	29.10	99.13	
0.244	25.75	0 0 6	25.75		154.5

Table 2. Summary of SAXD peaks of DPPE after the vacuum treatment for 30 min. Dashes denote that definite peak was not observed.

q (Å^{-1})	$d_{\rm obs}$ (Å)	$h\ k\ l$	$d_{\rm cal}$ (Å)	a (Å)	c (Å)
0.082	76.59	1 0 1	76.59	99.62	
0.107	58.18	0 1 2	59.81	99.38	
0.114	55.12	0 0 3	55.58		166.7
0.123	51.08	1 1 0	49.84	99.68	
-		0 2 1	41.87		
-		1 0 4	37.38		
-		0 1 5	30.94		
0.225	27.93	0 0 6	27.67		166.0

−120 °C and is in the disordered liquid state at room temperature [25]. The first two systems are mixture of NP and ZP, and the third system is a mixture of two ZPs as a reference sample.

The temperature composition phase diagram for the DPhPC/DPPC binary system is shown in Figure 4(a). In the high-temperature region, DPhPC and DPPC mix completely as one uniform liquid phase. By decreasing the temperature, the binary system undergoes a phase separation into coexisting two liquid phases. It should be noted that for $M_{\rm DPhPC} < 5\%$ ($M_{\rm DPhPC}$: mole fraction of DPhPC) a solid-liquid coexisting phase boundary is observed and pure DPPC shows a solid phase in the region of $T < 41$ °C [21]. In the phase diagram we show the fluorescence micrograph images of vesicles in the one-phase region and the two-phase region. Here the bright region and the dark region correspond to DPhPC-rich phase and DPPC-rich phase, respectively. In the one-phase region, the vesicle shows a homogeneous monotonic appearance, whereas in the coexisting liquid-liquid phase region, the vesicle has several circular liquid domains.

For the DPPE/DOPC binary system, the obtained phase diagram is shown in Figure 4(b). It should be noted that the binary systems with DPPE mole fraction $M_{\rm DPPE} > 60\%$ could not form GUVs, which may be due to its large negative spontaneous curvature. At high temperature, a mixture of DPPE and DOPC is in one

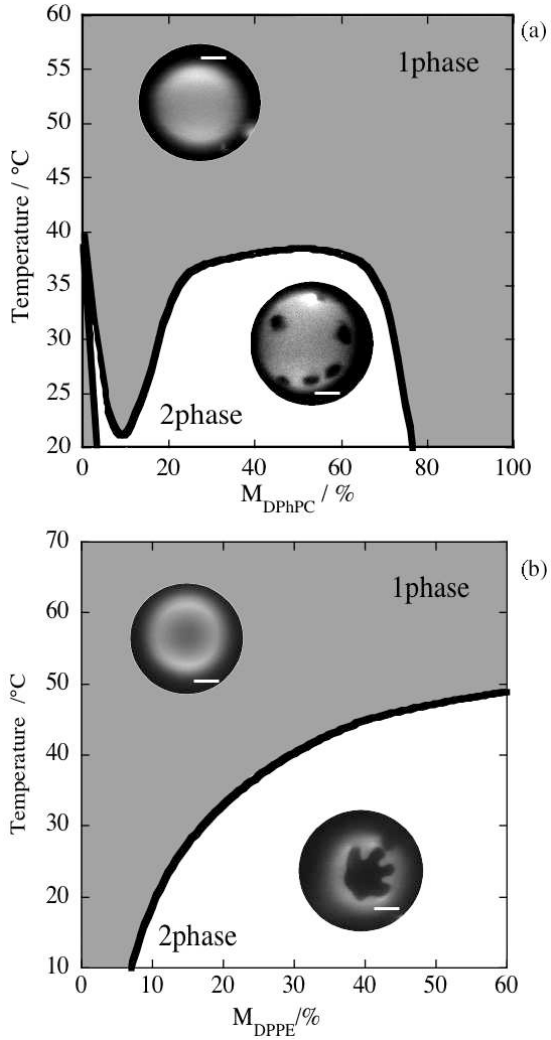

Fig. 4. Phase diagram of binary GUVs. Fluorescence micrograph images in figures show the appearance of vesicle at one-phase and two-phase region. Scale bars indicate 5 μm. (a) DPhPC/DPPC binary system and (b) DPPE/DOPC binary system. M_{DPhPC} and M_{DPPE} are mole fractions of DPhPC and DPPE, respectively.

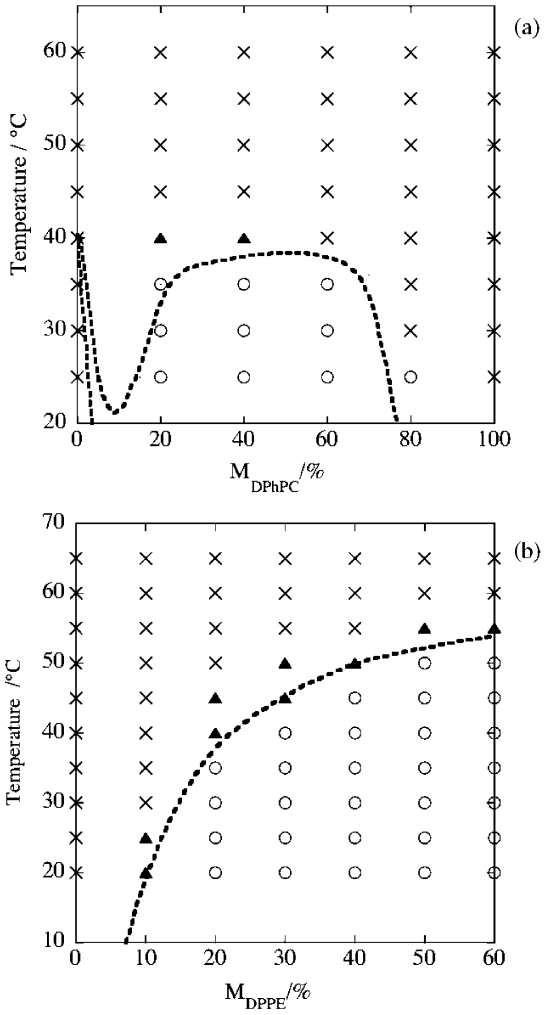

Fig. 5. Adhesion diagram of binary GUVs in the composition and the temperature space, (a) DPhPC/DPPC system and (b) DPPE/DOPC system. Circle, cross and triangle indicate adhesion, non-adhesion and boundary states, respectively. Dashed lines are phase boundaries.

uniform liquid phase. Between the melting temperatures of DPPE and DOPC, the system separates into coexisting solid and liquid phases. The immiscible boundary line approaches T_{m} of DPPE with the increase of M_{DPPE}. In the coexisting two-phase region, the vesicle has domains with complex shapes (Fig. 4(b)) compared with the circular liquid domains (Fig. 4(a)). The former has characteristic morphologies for solid domains [21]. Here the dark region and the bright region correspond to DPPE-rich phase and DOPC-rich phase, respectively.

The DPPC/DOPC binary system shows a similar phase diagram to the DPPE/DOPC binary system. At high temperature, DPPC and DOPC mix completely in a single homogeneous liquid phase. By decreasing the temperature, the system separates into a solid phase (rich in DPPC) and a liquid phase (rich in DOPC). The phase boundary approaches T_{m} of DPPC for $M_{\mathrm{DOPC}} \to 0\%$ and T_{m} of DOPC for $M_{\mathrm{DOPC}} \to 100\%$ (M_{DOPC}: DOPC mole fraction). The phase behavior of the DPPC/DOPC binary system agrees well with that in the literature [26,27].

3.3 Adhesion of binary GUVs

Based on the above phase diagrams, we examine the adhesion of the binary GUVs using the micro-manipulation method. Before we examined the adhesion of the binary vesicles, we confirmed that one-component GUVs composed of pure ZP (DPPC or DOPC) have no adhering ability in the temperature region from 20 to 60 °C.

The adhesion tests for the DPhPC/DPPC binary GUVs were performed at grid points in the temperature-composition space shown in Figure 5(a). Circles indicate that the GUVs adhere to each other at the corresponding compositions and temperatures, cross symbols mean that GUVs do not show the adhesion and triangles indicate

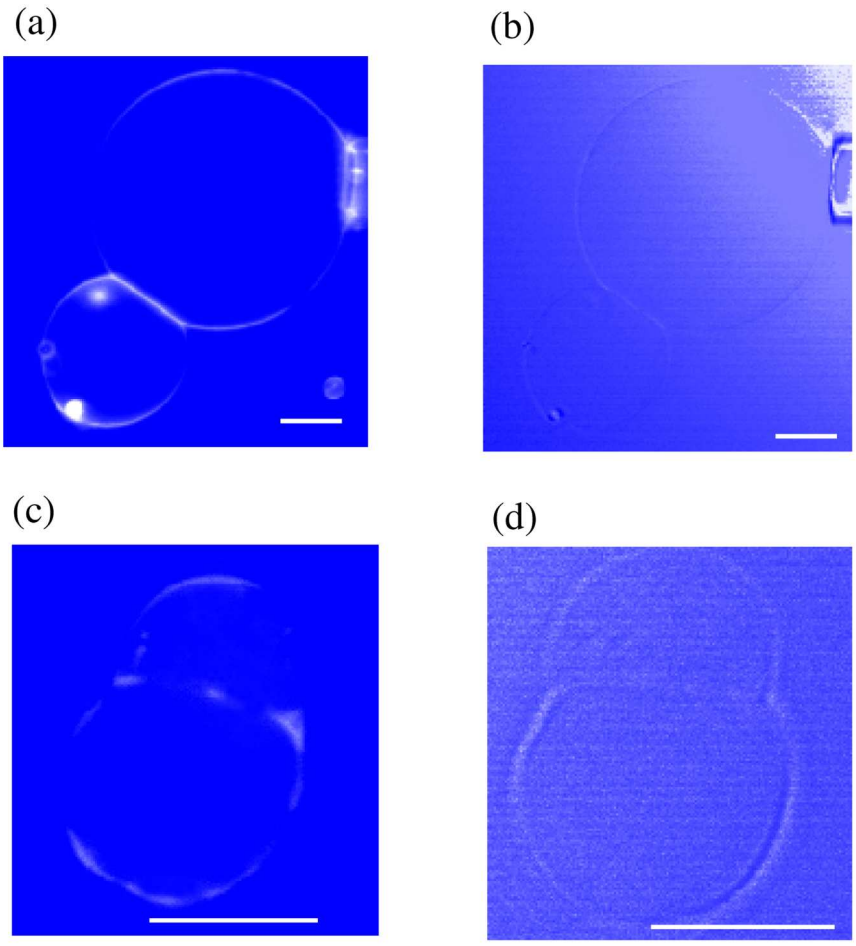

Fig. 6. Fluorescence microscope images of adhering GUVs for (a) DPhPC/DPPC and (c) DPPE/DOPC and corresponding confocal microscope images for (b) DPhPC/DPPC and (d) DPPE/DOPC. Scale bars indicate 10 μm.

the boundary region. The adhesion takes place only in the two-phase region of the binary system; the adhesion/non-adhesion boundary (Fig. 5(a)) agrees well with the immiscible boundary of the DPhPC/DPPC binary vesicles (Fig. 4(a)). Figure 5(a) clearly shows that GUVs composed of pure DPhPC ($M_{\mathrm{DPhPC}} = 100\%$) show no adhesion in the temperature region from 60 to 20 °C. Thus the formation of DPhPC domains plays a crucial role in the vesicle adhesion. In Figure 6(a) we show a confocal fluorescence cross-section image of the adhering DPhPC/DPPC binary vesicles dyed with TR-DHPE with a corresponding confocal image (Fig. 6(b)). The TR-DHPE is localized in the region rich in DPhPC and the region rich in DPPC is recognized as dark parts. The adhering part of the GUVs shows intense line compared with the other circumference of the GUVs. By taking into account the fact that the adhesion behavior of DPhPC/DPPC binary vesicles without TR-DHPE agrees with that of DPhPC/DPPC binary vesicles in the presence of TR-DHPE, we see that the fluorescence dye does not affect the present adhesion results significantly. From these experimental results we conclude that the DPhPC/DPPC binary GUVs adhere to each other through the region rich in DPhPC, *i.e.* the negative spontaneous curvature region.

We performed similar experiments for the DPPE/DOPC binary GUVs and results of the adhesion test are summarized in Figure 5(b). Again we obtained good agreement between the phase behavior (Fig. 4(b)) and the adhesion map (Fig. 5(b)), indicating the importance of the phase separation in the adhesion. In Figure 6(c) we show the confocal fluorescence cross-section image of adhering DPPE/DOPC binary GUVs dyed with TR-DHPE, where TR-DHPE is localized in the DOPC-rich phases. The fluorescence cross-section microphotograph image and the corresponding confocal image (Fig. 6(d)) clearly show that GUVs adhere to each other through the dark region, namely, DPPE solid domains with the negative spontaneous curvature.

Furthermore, we forced to separate the adhering vesicles using the micro-pipettes with high suction pressure $P \sim 500\,\mathrm{Pa}$ ($\tau \sim 33\,\mathrm{mN/m}$). In Figure 7 we show the snapshots of the forced separation experiments of adhering binary vesicles with the composition of DPPE/DOPC = 6/4 at 25 °C. By pulling one of the adhering vesicles, the opposing vesicle was stretched showing an hourglass shape as in Figure 7(b). Finally the opposing vesicle was ruptured and the adhering area was left on the pulling vesicle as a patch (Fig. 7(c)). Due to the smearing effect of

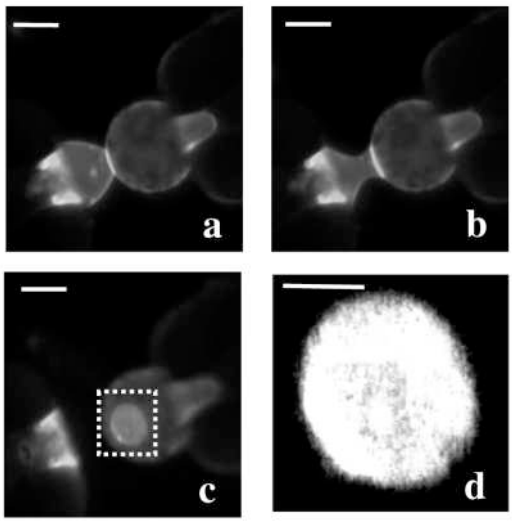

Fig. 7. Snapshots of forced separation experiments ($P \sim 500\,\mathrm{Pa}$) of adhering binary vesicles with the composition of DPPE/DOPC = 6/4 at 25 °C, (a) just after pulling the pipette away, (b) intermediate state where opposing vesicle was deformed to hourglass shape, and (c) opposing vesicle was ruptured and the adhering area was left on the pulling vesicle as a patch. Bars in (a), (b) and (c) indicates 15 μm. The enlarged high-contrast image of the dotted-square region in (c) is shown in (d). Bar in (d) indicates 7.5 μm.

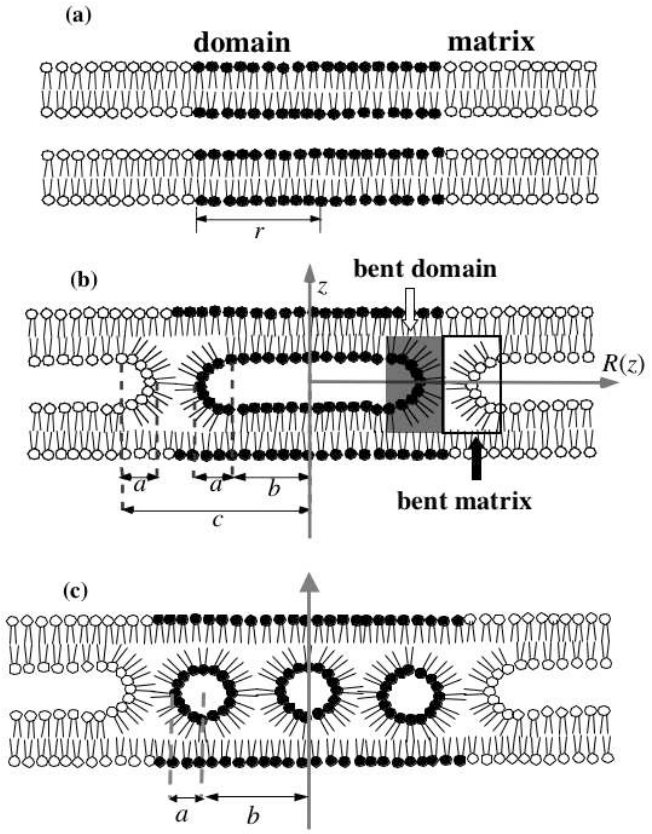

Fig. 8. Schematic representation of (a) parallel membrane (non-hemifusion) state, (b) hemifusion state with pancake shape and (c) hemifusion state with spherical shape. Coordinates for free-energy calculation are shown in (b) and (c).

fluorescence from the surrounding matrix, the patch seems to be bright, but the high contrast image of this patch (Fig. 7(d)) shows that its center region is occupied by the dark DPPE-rich region. Thus the adhesion through the negative spontaneous curvature region has a strong adhesion force.

On the other hand, DPPC/DOPC binary GUVs did not show adhesion of GUVs in the observed temperature-composition space, indicating that the domains with zero spontaneous curvature have no adhesion ability even in the coexisting two-phase region. These results clearly show that the adhesion takes place for the binary GUVs composed of NP and ZP through domains rich in NPs and is independent of whether the domain is in liquid or solid phase.

3.4 Lipid transfer observation

The essential point of our observations is that the adhesion takes place only through the domains rich in NPs. So far the membrane adhesions have been explained from the view points of the specific interactions using the ligand and receptor molecules embedded in membranes or the interplay among the generic interactions [1–9,24]. Since in our case no specific molecules are added to the systems, one of the plausible explanations is the interplay between the generic interactions. Thus if DPPE and DPhPC have large adhesion energies (energy at the position of the interaction potential minima), the domains rich in DPPE (or DPhPC) adhere with the domains on opposing vesicles. It is reported that DPPE has the adhesion energy of $-0.7 \approx -0.8 \times 10^{-3}\,\mathrm{J/m^2} = -0.07 k_\mathrm{B}T/\mathrm{molecule}$ [5,7], which is larger than that of DPPC ($-0.15 \times 10^{-3}\,\mathrm{J/m^2}$) [5]. Although the adhesion energy of DPhPC has not been reported in the literatures, the interplay among the generic interactions may be one model to explain the observed adhesions. In our experiments, however, the adhesion took place only for the coexistence phase region and we never observed adhesion for the one component GUVs composed of pure NP (DPhPC). The coupling between generic interactions and phase separation has been addressed by theoretical [28,29] and simulation approaches [30–32]. Komura and Andelman proposed a phenomenological model for the unbinding transition of multicomponent fluid membranes and showed the phase separation coupled with the bound and unbound membrane states [29]. The theoretical phase diagram predicts that the adhesion takes place not only in the two-phase region but also in the one-phase region, which cannot describe the observed adhesion behavior. Therefore, it is worthwhile to consider another model to explain the experimental results. In this paper we propose a hemifusion model where the negative spontaneous curvature domain forms the hemifusion structure with the apposing negative spontaneous curvature domain. In Figure 8 we show the schematic representations of the hemifusion models: (a) parallel membrane (non-adhesion) state,

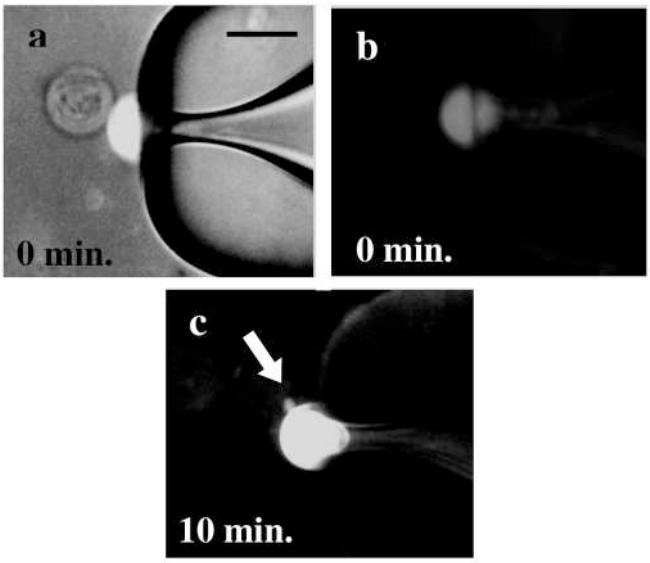

Fig. 9. Two adhering GUVs composed of DPPE/DOPC (= 60/40) in fluorescence lipid transfer experiment, (a) phase contrast + fluorescence image and (b) fluorescence image for adhering GUVs just after contacting. Bright GUV is a fluorescent labeled GUV and non-labeled GUV is positioned at the left side of the labeled GUV (detected by phase contrast image in (a) and not seen in (b)). After 10 minutes, fluorescent signal appears in non-labeled GUV in the neighborhood of the contacting area (indicated by an arrow) in the fluorescence image (c).

(b) hemifusion (adhesion) state with a pancake shape and (c) hemifusion state with a spherical shape. In the hemifusion states, the outer leaflets of both vesicles' bilayers are merged whereas the inner leaflets remained independent and the domain boundary between NP-rich and ZP-rich regions is eliminated.

In order to examine the hemifusion model, we performed fluorescence lipid transfer experiments using two types of DPPE/DOPC binary GMVs. The first type contained fluorescent labeled lipids TR-DHPE and the second type had no fluorescence. Two phase separating GMVs of different types were brought into adhesion by means of the micro-manipulation (Fig. 9(a): phase contrast + fluorescence microscope image). Just after the adhesion, the labeled vesicle showed a fluorescent signal from the matrix rich in DOPC whereas the non-labeled GMV could not be detected by the fluorescent microscope observation as shown in Figure 9(b). Slightly after the adhesion (several minutes), a fluorescent signal was observed in the neighborhood of the contact area on the non-labeled GMV as shown by an arrow in Figure 9(c). Unfortunately the photo images are somewhat obscure, because the fluorescence from the transferred lipids is fairly weak and localized to the parts of the non-labeled GMV. Then we repeated the lipid transfer experiments several times and confirmed the reproducibility of fluorescence lipid transfer by eye observations.

The main argument on the lipid transfer experiments may be the migration of fluorescent lipids between opposing bilayers across the water layer. In this case it would not need hemifusion. Here we estimate the diffusion constant of typical saturated phospholipids, DPPC, across the water layer using a time-resolved small-angle neutron-scattering (TR-SANS) technique [33]. This is based on the fact that scattering length densities (SLDs) are significantly different between vesicles consisting of hydrogenated and deuterated phospholipids and that the lipid exchange between these vesicles reduces the difference in SLD with time. The rough estimated diffusion constant of DPPC across the water layer at 25 °C is $D < 1 \times 10^{-25}\,\mathrm{m}^2/\mathrm{s}$, which is quite slow compared with the time scale of our lipid exchange experiments of ~ 10 min. Then we believe that the fluorescent lipids transfer to the non-labeled vesicle through the hemifused outer leaflets and not by the migration across the water layer. Details of this lipid exchange experiments using TRSANS will be described in a forthcoming paper. Thus the labeled lipids transfer to the adhering non-labeled GMV through the hemifusion of the outer leaflets of the matrix. This strongly supports the hemifusion model to account for the adhesion of binary GUVs containing NP.

4 Discussion

Here we discuss the stability of the hemifusion state using a membrane elasticity model. In the hemifusion model, the adhesion may take place in order to decrease the bending energy of the flat membrane with negative spontaneous curvature and eliminate the boundary energy between the domain and matrix. The total energies of adhering membranes and non-adhering membranes, which are expressed by a sum of the curvature elasticity and boundary energy, is

$$F = 2\kappa \int (H - H_0)^2 \mathrm{d}S + 2\sigma \oint \mathrm{d}l, \tag{8}$$

where H is the mean curvature, H_0 the spontaneous curvature, and σ the line tension between the domain and matrix. As shown in Figure 8, in the hemifusion state, the outer leaflets of both vesicles' bilayers are merged whereas the inner leaflets remain independent. We calculate the energy of the outer leaflets to compare the total energy between the hemifusion state and the parallel membrane (non-hemifusion) state. It should be noted that the deformation takes place not only in the domain side (bent domain) but also in the matrix adjacent to the domain boundary (bent matrix). For convenience we deal with the pancake shape hemifusion case shown in Figure 8(b), where the domains have circular shape and adhesion takes place between opposing domains with the same area. In order to calculate the bending energy in equation (8) we introduce a cylindrical coordinate as shown in Figure 8(b). For a surface given in terms of the local radius, $R(z)$, the area element is

$$\mathrm{d}S = 2\pi R(z)\sqrt{1 + R_z(z)^2}\mathrm{d}z, \tag{9}$$

where the subscript denotes partial derivative, and the

mean curvature H is expressed by

$$H = \frac{RR_{zz} - 1 - R_z^2}{2R(1+R_z^2)^{3/2}}\,. \tag{10}$$

We consider two situations according to the experiments, one is the membranes with negative spontaneous curvature domain ($H_0 = -1/a$) and the zero spontaneous curvature matrix ($H_0 = 0$), and the other is the membranes with zero spontaneous curvature domain and zero spontaneous curvature matrix.

First we deal with the NP and ZP mixture membranes. For the hemifusion membrane case, the boundary between domain and matrix is eliminated by the formation of the hemifusion state and the total energy is expressed by a sum of the bending energies of the flat domain region, bent domain region, and bent matrix region. For the bent domain (Fig. 8(b)), the local radius $R(z)$ of the domain boundary has the form

$$R(z) = b + \sqrt{a^2 - z^2} \tag{11}$$

and for bent matrix the boundary is expressed by

$$R(z) = c - \sqrt{a^2 - z^2}\,. \tag{12}$$

Then the total energy is given by

$$\begin{aligned} F_{\rm NZ}^{\rm hemi} = {} & 4\pi\kappa_1\frac{b^2}{a^2} + 2\kappa_1\left(\frac{\pi^2 b^2}{2a\sqrt{b^2-a^2}} - \frac{\pi b^2 \arctan\left(\frac{a}{\sqrt{b^2-a^2}}\right)}{a\sqrt{b^2-a^2}}\right) \\ & + 2\kappa_2\left(-4\pi + \frac{7\pi^2 c^2}{2a\sqrt{c^2-a^2}} + \frac{\pi c^2 \arctan\left(\frac{a}{\sqrt{c^2-a^2}}\right)}{a\sqrt{c^2-a^2}}\right), \end{aligned} \tag{13}$$

where κ_1 and κ_2 are the bending rigidities of domain monolayer with $H_0 = -1/a$ and matrix monolayer with $H_0 = 0$, respectively. In our experiments, the domain size ($b \sim c \sim 5\,\mu$m) is much larger than the inter-membrane distance ($a \sim 10\,$nm), then the total energy can be approximated as

$$F_{\rm NZ}^{\rm hemi} \sim \frac{\pi^2}{2}(2\kappa_1 + 7\kappa_2)\frac{b}{a} + 4\pi\kappa_1\frac{b^2}{a^2}\,. \tag{14}$$

On the other hand, for the parallel membrane (non-hemifusion) case, the total energy is a sum of the bending energy and the boundary energy. The radius of the circular domain, r, is related to the geometrical parameters a and b in the hemifused domain via the area conservation constraint

$$r = \sqrt{2a^2 + b^2 + \pi ab}\,. \tag{15}$$

Then the total energy is given by

$$\begin{aligned} F_{\rm NZ}^{\rm para} &= 4\pi\kappa_1\left(2 + \pi\frac{b}{a} + \frac{b^2}{a^2}\right) + 2\pi\sigma\sqrt{2a^2 + b^2 + \pi ab} \\ &\sim 4\pi\kappa_1\left(\pi\frac{b}{a} + \frac{b^2}{a^2}\right) + 2\pi\sigma b, \end{aligned} \tag{16}$$

where σ is the line tension between the negative spontaneous curvature domain and the zero spontaneous curvature matrix. The formation of the hemifusion state is determined by the balance of the boundary energy and bending energy.

Next we address the ZP and ZP mixture membranes. In this case the total energy for the hemifusion state is given by

$$\begin{aligned} F_{\rm ZZ}^{\rm hemi} = {} & 2\kappa_3\left(4\pi + \frac{\pi^2 b^2}{2a\sqrt{-a^2+b^2}} - \frac{\pi b^2 \arctan\left(\frac{a}{\sqrt{-a^2+b^2}}\right)}{a\sqrt{-a^2+b^2}}\right) \\ & + 2\kappa_2\left(-4\pi + \frac{7\pi^2 c^2}{2a\sqrt{-a^2+c^2}} + \frac{\pi c^2 \arctan\left(\frac{a}{\sqrt{-a^2+c^2}}\right)}{a\sqrt{-a^2+c^2}}\right) \\ & \sim \frac{\pi^2}{2}(2\kappa_3 + 7\kappa_2)\frac{b}{a}\,, \end{aligned} \tag{17}$$

where κ_3 is the bending elasticity of domain monolayer with $H_0 = 0$. The total energy for the parallel membrane state is expressed by the boundary energy only and given by

$$F_{\rm ZZ}^{\rm para} = 2\pi\sigma'\sqrt{2a^2 + b^2 + \pi ab} \sim 2\pi\sigma' b, \tag{18}$$

where σ' is the line tension between the zero spontaneous curvature domain and matrix.

Thus the total energy difference between the hemifusion state and the parallel membrane state for NP and ZP binary membranes is expressed by

$$\Delta F_{\rm NZ} = F_{\rm NZ}^{\rm para} - F_{\rm NZ}^{\rm hemi} = 4\pi^2\kappa_1\frac{b}{a} + 2\pi\sigma b - \frac{\pi^2 b}{2a}(2\kappa_1 + 7\kappa_2) \tag{19}$$

and for ZSCP and ZSCP binary membranes the energy difference is given by

$$\Delta F_{\rm ZZ} = F_{\rm ZZ}^{\rm para} - F_{\rm ZZ}^{\rm hemi} = 2\pi\sigma' b - \frac{\pi^2 b}{2a}(2\kappa_3 + 7\kappa_2). \tag{20}$$

From the literature, the bending modulus of bilayer membrane, κ, typically has a value of $\sim 10^{-19}\,$J [34] (DOPC: $0.8 \times 10^{-19}\,$J [34], DPPC: $0.5 \times 10^{-19}\,$J for liquid disordered phase [35] and $\sim 1 \times 10^{-19}\,$J for ordered phase [36], and DPhPC: $1.2 \times 10^{-19}\,$J [35]) and the line tension, σ, is estimated as the order of $\sim 10^{-11}\,$N [37]. For the numerical calculations, we adopted the following values: $\kappa_1 \sim \kappa_2 \sim \kappa_3 \sim \frac{1}{2} \times 10^{-19} = 5 \times 10^{-20}\,$J and $\sigma \sim \sigma' \sim \frac{1}{2} \times 10^{-11} = 5 \times 10^{-12}\,$N (factor 1/2 accounts for the monolayer membranes). For the NP and ZP binary membranes, we obtained $\Delta F_{\rm NZ} = 3.8 \times 10^{-17}\,$J, *i.e.* $F_{\rm NZ}^{\rm para} > F_{\rm NZ}^{\rm hemi}$, indicating that the membranes prefer to form the hemifusion state. On the other hand, for the ZP and ZP binary membranes, we obtained $\Delta F_{\rm ZZ} = -86 \times 10^{-17}\,$J, *i.e.* $F_{\rm ZZ}^{\rm para} < F_{\rm ZZ}^{\rm hemi}$, indicating that the membranes prefer the separated membrane state. These theoretical predictions agree well with the experimental observations. It is worthwhile to note that $\Delta F_{\rm NZ}$ is larger than $\Delta F_{\rm ZZ}$ by $4\pi^2\kappa_1 b/a$, which determines the sign of the total energy differences, $\Delta F_{\rm NZ}$ and $\Delta F_{\rm ZZ}$. This term originates from the bending of the negative spontaneous curvature domain. Thus the

formation of negative spontaneous curvature domain is responsible for the observed adhesion behavior.

In the model calculation described above, we adopted the pancake shape model for the hemifusion state. Of course we can consider other hemifusion shapes such as spherical hemifusion shape, where the outer leaflets form spheres with the curvature of $H_0 = 1/a$ as shown in Figure 8(c). In this case, the total energy for the spherical hemifusion is expressed by

$$^{\rm sp}F_{\rm NZ}^{\rm hemi} \sim \frac{7\pi^2}{2}\frac{b}{a}\kappa_2\,, \tag{21}$$

where the geometrical parameters a and b are defined in Figure 8(c). For the spherical hemifusion case, the bending energy merit of the negative spontaneous curvature membranes is more emphasized and the hemifusion is encouraged compared with the case of the pancake hemifusion. Thus the pancake shape is the least stable shape to achieve the hemifusion and the hemifusion models can explain the observed adhesion behavior.

5 Conclusion

In this study we found the adhesion of the binary GUVs composed of the NP and ZP induced by the phase separation. In the one-phase region, the GUVs do not show adhesion but in the coexisting two-phase region the GUVs show adhesion through the domains rich in NPs. Based on the experimental results we propose the phase separation induced hemifusion model where the outer leaflets of the bilayers merge at the boundary of the negative spontaneous curvature domains. The fluorescence lipid transfer experiment strongly supports the hemifusion model. The model energy calculations show that the formation of the negative curvature domain is crucial for the stabilization of the hemifusion state. In contrast to the adhesion of membrane induced by the specific interactions such as ligand-receptor pairs or the interplay of the generic interactions, a unique feature of this system is that the adhesion of GUVs is controlled by changing the temperature, which may bring a new pathway of membrane technology.

We thank Prof. Toshihiro Kawakatsu (Tohoku University) for valuable discussions. This work was supported by KAKENHI (Grant-in-Aid for Scientific Research) on Priority Area "Soft Matter Physics" from the Ministry of Education, Culture, Sports, Science and Technology of Japan.

References

1. R. Simson, E. Sackmann, in *Physical Chemistry of Biological Interfaces* (Marcel Dekker, Inc., New York, 2000).
2. L.J. Lis, M. McAlister, N. Fuller, R.P. Rand, V.A. Parsegian, Biophys. J. **37**, 657 (1982).
3. E. Evans, D. Needham, Faraday Discuss. Chem. Soc. **81**, 267 (1986).
4. R. Lipowsky, S. Leibler, Phys. Rev. Lett. **56**, 2541 (1986).
5. R.P. Rand, V.A. Parsegian, Biochem. Biophys. Acta **988**, 351 (1989).
6. J.O. Rädler, T.J. Feder, H.H. Strey, E. Sackmann, Phys. Rev. E **51**, 4526 (1995).
7. T.J. McIntosh, S.A. Simon, Langmuir **12**, 1622 (1996).
8. J.F. Nagel, S. Tristran-Nagel, Biochim. Biophys. Acta **1469**, 159 (2000).
9. Although the properties of the binding-unbinding transition cannot be described by a simple superposition of the generic interactions, it gives a reasonable estimation of the effective inter-membrane potential [4].
10. M.M. Kozlov, V.S. Markin, Biofizika **28**, 255 (1983).
11. P. I. Kuzumin, J. Zimmerberg, Y.A. Chizmadzhev, F.S. Cohen, Proc. Natl. Acad. Sci. U.S.A. **98**, 7235 (2001).
12. V. Markin, J. Albanesi, Biophys. J. **82**, 693 (2002).
13. S. May, Biophys. J. **83**, 2969 (2002).
14. H. Noguchi, M. Takasu, J. Chem. Phys. **115**, 9547 (2001).
15. S.J. Marrink, A.E. Mark, J. Am. Chem. Soc. **125**, 11144 (2003).
16. J. Heuvingh, F. Pincet, S. Cribier, Eur. Phys. J. E **14**, 269 (2004).
17. L. Yang, H.W. Huang, Science **297**, 1877 (2002).
18. L. Yang, H.W. Huang, Biophys. J. **84**, 1808 (2003).
19. J.P. Reeves, R.M. Dowben, J. Cell. Physiol. **73**, 49 (1969).
20. D. Needham, E. Evans, Biochemistry **27**, 8261 (1988).
21. S.L. Veatch, S.L. Keller, Biophys. J. **85**, 3074 (2003).
22. R. Kwok, E.A. Evans, Biophys. J. **35**, 637 (1981).
23. W. Rawicz, K.C. Olbrich, T. McIntosh, D. Needham, E. Evans, Biophys. J. **79**, 328 (2000).
24. W. Helfrich, Z. Naturforsch. **33a**, 305 (1978).
25. H. Lindsey, N.O. Petersen, S.I. Chan, Biochim. Biophys. Acta. **555**, 147 (1979).
26. S.L. Veatch, S.L. Keller, Biophys. J. **85**, 3074 (2003).
27. B.R. Lentz, Y. Barenholz, T.E. Thompson, Biochemistry **15**, 4529 (1976).
28. R. Lipowsky, Phys. Rev. Lett. **77**, 1652 (1996).
29. S. Komura, D. Andelman, Europhys. Lett. **64**, 844 (2003).
30. T.R. Weikl, R.R. Netz, R. Lipowsky, Phys. Rev. E **62**, R45 (2000).
31. T.R. Weikl, R. Lipowsky, Phys. Rev. E **64**, 011903 (2001).
32. T.R. Weikl, D. Andelman, S. Komura, R. Lipowsky, Eur. Phys. J. E **8**, 59 (2002).
33. M. Nakano, M. Fukuda, T. Kudo, H. Endo, T. Handa, Phys. Rev. Lett. **98**, 238101 (2007).
34. H.P. Duwe, E. Sackmann, Physica A **163**, 410 (1990).
35. D. Marsh, Chem. Phys. Lipids. **144**, 146 (2006).
36. We estimated the bending modulus of DPPC in order phase based on Milner and Safran method (S.T. Milner, S.A. Safran, Phys. Rev. A **36**, 4371 (1987)) by means of a neutron spin echo and a small-angle neutron scattering measurement.
37. R. Lipowsky, J. Phys. II **2**, 1825 (1992).